

Local and Remote Forcing Factors of Heatwave in India – A Reanalysis and Adjoint model based study

Abhirup Banerjee^{*1}, Armin Koehl¹, Frank Lunkeit², and Detlef Stammer¹

¹Institut für Meereskunde, Centrum für Erdsystemforschung und Nachhaltigkeit, Universität Hamburg, Hamburg, Germany

²Meteorologisches Institut, Centrum für Erdsystemforschung und Nachhaltigkeit, Universität Hamburg, Hamburg, Germany

This work has been submitted to the Journal of Climate. Copyright in this work may be transferred without further notice.

Abstract

Continental heatwaves can dramatically impact ecosystems and societies, e.g., by leading to excess mortality, wildfires, and harvest failures. With a warming climate, their impacts potentially intensify globally, but the Indian subcontinent appears to be particularly vulnerable to such extreme events. In this study, we use reanalysis and the adjoint of the atmospheric model, PlaSim, to identify drivers of heatwaves occurring April and May over north-central India. Reanalysis results suggest that the existence of high temperatures in the study region is highly sensitive to the low local soil moisture which is observed weeks before a heatwave commences. Soil moisture variability in northern India is influenced by moisture transport from the west during winter–spring. Preceding dry soil moisture conditions can be associated with a ‘persistent jet’ conditions linked to atmospheric dynamical changes in the North Atlantic region. An associated northward shift in the upper tropospheric zonal wind occurs approximately a month prior to the heatwaves, influencing the area and intensity of western disturbances embedded in the jet stream. This weakens the moisture flow from the north of the Arabian Sea, further reducing soil moisture levels and creating conditions conducive to heatwaves. An adjoint sensitivity analysis and forward model perturbation experiments confirm the causal relationships for the proposed heatwave development mechanism over north-central India, identifying the remote influence of North Atlantic sea surface temperature variability on extreme temperatures in India. Our findings highlight the complex interplay of local and remote factors in heatwave development over India.

*Corresponding author: abhirup.banerjee@uni-hamburg.de

1 Introduction

Continental heatwaves (HWs) are meteorological phenomena characterized by prolonged periods of abnormally high temperatures that usually persist for days to weeks. These extreme events present a formidable hazard to ecosystems and societies, resulting in substantial economic losses and an alarming increase in mortality rates (Zuo et al., 2015; García-León et al., 2021; Campbell et al., 2018). As an example, at the time of writing, the losses of life in India during 2024 already exceed 40,000 due to suspected heat stroke cases, and more than 100 heat-related deaths¹. The influence of anthropogenic warming on the occurrence of HWs is evident from the increment in their occurrence and in their increased intensity (Russo et al., 2014; Domeisen et al., 2023). A significant upward trajectory in both the frequency and the severity of heat events is observed in the Indian subcontinent (Panda et al., 2017) posing significant risk for public health and societal well-being (Debnath et al., 2023; Im et al., 2017; Mazdiyasnani et al., 2017; de Bont et al., 2024).

The development of HWs over India is a multifaceted process influenced by a range of factors, including anomalies in both regional and local atmospheric conditions (Ratnam et al., 2016; Dubey et al., 2021). In addition, large-scale teleconnections such as the El Niño-Southern Oscillation (Hari et al., 2022; Lekshmi and Chattopadhyay, 2022; Pai and Nair, 2022; Kumar et al., 2023), oceanic influences (Pai et al., 2013; Vittal et al., 2020), and other regional factors (Ganeshi et al., 2020; Satyanarayana and Rao, 2020) also play a significant role in the occurrence of HWs across India. Specifically, Vittal et al. (2020) demonstrated that the Atlantic Ocean sea surface temperature (SST) had a greater influence on temperature extremes over India compared to the Pacific and Indian Ocean SST during the 1961–2010 period, with this influence being exacerbated by anthropogenic forcing. However, the detailed knowledge of the necessary conditions and the sequence of processes leading to HWs remains limited. Predicting HWs remains therefore difficult and relies primarily on statistical relations rather than the knowledge of physical processes.

Previous studies have shown that HWs are strongly associated with high-pressure systems and anticyclonic circulation, leading to moisture subsidence and clear skies that support heating (Barriopedro et al., 2023; Perkins, 2015; Horton et al., 2016; Pfahl and Wernli, 2012). These summer temperature extremes can be amplified or dampened by land-atmosphere interactions. Numerous studies have shown that land-atmosphere interactions can amplify HWs (Lorenz et al., 2010; Jaeger and Seneviratne, 2011; Vogel et al., 2017) with soil moisture (SM) being a key mediator of these interactions (Seneviratne et al., 2010; Horton et al., 2015). Deficits in SM have been linked to specific extreme heat events also in the United States and Europe (Fischer et al., 2007b; Wehrli et al., 2019). In the context of temperature extremes in India, Ganeshi et al. (2020, 2023) have reported the role of SM variability in a warming climate.

In recent years, the region of north-central India (NCI) has been particularly exposed to HWs and experiences a rising trend in the occurrence of HWs (Rohini et al., 2016, 2019). During winter–spring, northwestern India receives moisture primarily from the north of the Arabian Sea. This is associated with ‘western disturbances’ (WDs) which are cyclonic storms embedded in the subtropical westerly jet (SWJ) (Yadav et al., 2012; Hunt et al., 2018a; Hunt, 2024; Baudouin et al., 2021). The variability in moisture transport over northern India during this period is generally linked to fluctuations in the intensity and frequency of WDs (Hunt et al., 2024). More details about WDs can be found in Hunt et al. (2018b).

In this paper, we identify the potential contribution of local soil moisture conditions to the development of HWs during April and May over NCI, and the moisture dynamics in the preceding winter–spring which lead to such conditions. Specifically, we seek the answer to the question of what are the anomalous changes in the large-scale circulation patterns during winter–spring leading to drier SM which in turn creates conditions ideal for HW development during summer. We combine reanalysis-based investigations with an adjoint sensitivity analysis via the adjoint of the atmospheric model PlaSim (Fraedrich et al., 2005; Blessing et al., 2014) which complement each other in identifying the distinctive precursory features of different climate variables prior to HWs and also unravel the possible causal relationships among them. Such a holistic approach offers a comprehensive understanding of the physical mechanism underlying HW developments over NCI. Understanding the preconditions of HWs is crucial for their accurate prediction, preparation, and response, as such factors can either intensify or alleviate these extreme events.

The remainder of the article is organized as follows. In Section 2, we introduce the methodology and data sets

¹<https://www.reuters.com/world/india/unrelenting-heatwave-kills-five-indian-capital-2024-06-19/>

used. This includes the definition of HW events and the description of the model PlaSim and its adjoint used in this study. In Section 3, we present our findings from reanalysis data, followed by those from the adjoint-sensitivity study and lastly from the model forward run experiments provided in Section 4. Concluding remarks are provided in Section 5.

2 Methodology

Several definitions of HWs exist in the literature (Barriopedro et al., 2023). This study is based on the HW indices (HW_t) over north-central India (NCI, $22^\circ - 31^\circ\text{N}$, $70^\circ - 77^\circ\text{E}$) provided by the India Meteorological Department (IMD)². To compute the temperature anomaly associated with HWs over India, we use the $1^\circ \times 1^\circ$ gridded maximum temperature (Tmax) daily data provided by IMD (Srivastava et al., 2009) which we accessed using IMDLIB python package (Nandi and Patel, 2020). To detect HW event in PlaSim, we considered when temperature (2m temperature, $T2m$) is above the 90th percentile for at least 5 consecutive days. A typical example of a NCI HW pattern in PlaSim is shown in Figure 1a representing the composites of $T2m$.

To analyze the state of the atmosphere and its variability surrounding HW events between April and May over the period of 1980 to 2022, a detrended standardized composite anomaly and Empirical Orthogonal Function (EOF) analysis (Dawson, 2016) of different variables are used. For atmospheric variables, we use the NCEP-NCAR Reanalysis 1 data (Kalnay et al., 2018). GLEAM v3.8a daily data is used for surface level soil moisture (Martens et al., 2017). With respect to sea surface temperature data, the NOAA Extended Reconstructed sea surface temperature data (V5) data is used (Huang et al., 2017). The dynamics of moisture transport associated with HWs will also be analyzed using the western disturbances (WDs) catalogue provided by Hunt and Zaz (2023) wherein the authors identified the regions with positive vorticity by analyzing the mean relative vorticity within 450-300 hPa and linked those regions based on a set of physical constraints.

Adjoint sensitivities of Indian HWs will be analyzed to infer mechanisms that potentially can contribute to a HW development. Subsequently, our findings from both the reanalysis and adjoint sensitivity studies will be tested through forward perturbation experiments. For both steps, an intermediate complexity climate model PlaSim (Fraedrich et al., 2005) is being used implemented globally with $5.6^\circ \times 5.6^\circ$ horizontal resolution and 10 vertical levels. The details and the parameters of the model can be found here³.

The cost function is defined as the area weighted mean of daily mean 2m air temperature ($T2m$) for each of the HW onset (day 0) in PlaSim as depicted by the black rectangle in Figure 1a,

$$J = \frac{\int_A T2mW dA}{\int_A W dA} \quad (1)$$

Here dA is the area of the black rectangle in the Figure 1a; the weighting matrix W is shown in Figure 1b.

The PlaSim adjoint is being generated using the automatic differentiation tool TAF (Blessing et al., 2014; Lyu et al., 2018). Adjoint models calculate the sensitivities of a cost function to various controls, such as initial and boundary conditions, revealing the non-local (in space and time) influence of model parameter on the specified cost function; examples of adjoint sensitivity analyses can be found by (Marotzke et al., 1999; Stammer et al., 2018). Stammer et al. (2018); Köhl and Vlasenko (2019) used the adjoint of PlaSim coupled to the MITgcm (called the CESAM model) to study the sensitivity of temperatures over norther Europe to North Atlantic parameters.

The uncoupled PlaSim adjoint is being used here to find the sensitivity of extreme temperature shown in Figure 1a and defined in eq.(1) with respect to other local and non-local atmospheric and land surface parameters, such as surface temperature, soil moisture or atmospheric transports. Since adjoint sensitivities are prone to developing fast-growing unstable modes limiting the length of the application period, Gaussian filters are used to dampen the fastest growing modes causing local spikes in the adjoint sensitivities and extend the window to some extent (Stammer et al., 2018). To obtain adjoint sensitivities to the above cost function eq.(1), the adjoint model is integrated backward in time. Due to the exponentially growing modes in the backward (in time) running adjoint model, we restrict our sensitivity analysis to 6 days backward from the occurrence of a HW.

²https://imd pune.gov.in/Reports/Met_Monograph_Cold_Heat_Waves.pdf

³<https://www.mi.uni-hamburg.de/en/arbeitsgruppen/theoretische-meteorologie/modelle/plasim.html>

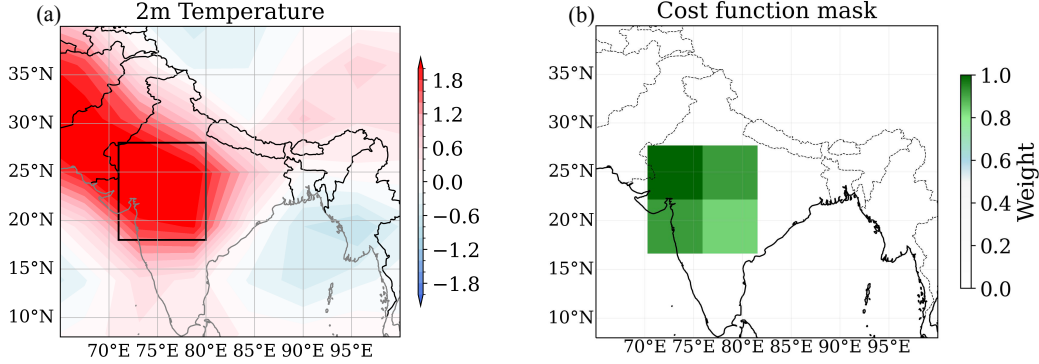


Figure 1: (a) Temperature anomaly [$^{\circ}\text{C}$] associated to the HWs over NCI in PlaSim. (b) Weighted mask used to compute the cost function.

Our analysis examines the sensitivity of extreme high temperatures with respect to the sea surface temperature (SST), upper tropospheric zonal wind (U_{wnd}), and soil moisture (SM). To this end we run the PlaSim model and its adjoint forward and backward for six distinct heatwave (HW) events, each corresponding to a different model year. We constructed the ensemble sensitivity by running the model backward using six independent initial conditions. The adjoint sensitivities presented below are expressed as ensemble means of these individual runs.

3 Unveiling the NCI Heat Wave Dynamics: Reanalysis-based study

Our study begins by examining the atmospheric conditions linked to heatwaves in the NCI region (black rectangle in Figure 2a), utilizing NCEP-NCAR 1 reanalysis data. Figure 2 (b-g) shows the standardized composite anomalies of various atmospheric parameters such as Figure 2a daily maximum temperature (T_{max}), Figure 2b mid-tropospheric geopotential height (Z_{500}), Figure 2c vertically integrated moisture transport (IVT), Figure 2d upper tropospheric zonal wind (U_{200}) and Figure 2e soil moisture (SM), all occurring at the time of HW onset. The figure shows that, coinciding with the HWs, a high-pressure system develops over India (Figure 2b). Consistent with Ratnam et al. (2016); Rohini et al. (2016), this pressure anomaly is associated with anticyclonic downward motion of air masses, producing dry air and reducing moisture flow over India (Figure 2c). Figure 2d suggests a simultaneous northward shift in zonal wind at 200 hPa (U_{200}) with respect to climatology (solid black contours denote April–May U_{200} climatology).

As low soil moisture can influence the atmospheric circulation patterns through land-atmospheric feedback (Fischer et al., 2007b; Koster et al., 2016), in Figures 2 (f - h) we plot the evolution of the composites of the anomalous SM prior to the HW events at NCI. Generally, a strong relationship between SM and surface temperature can be observed over Indian subcontinent (Berg et al., 2015; Miralles et al., 2012; Joy and Satheesan, 2022; Koster et al., 2006). Reduced soil moisture decreases latent heat flux while increasing surface warming; which in turn amplifies sensible heat flux through diabatic heating, leading to elevated air temperatures (Alexander, 2011; Röthlisberger and Papritz, 2023; Fischer et al., 2007a; Rohini et al., 2016; Seneviratne et al., 2010; Perkins, 2015). Low SM conditions are evident as early as 3 weeks prior to the occurrence of a HW. As we approach the HW onset (HW_t), dry moisture conditions intensify. Such persistent dry soil moisture (SM) conditions can also be linked to low late winter–spring precipitation (February to April) as shown in Figure A1.

To gain further insight into the factors contributing to low SM leading to subsequent HW development in NCI, we investigate the moisture dynamics in the context of large-scale circulations during the period of February to April (FMA). The moisture transport during winter–spring is generally associated with the intensity and position of the ‘western disturbances’ (WDs) (Hunt et al., 2018a; Hunt and Zaz, 2023; Yadav et al., 2012). The climatology of Western Disturbances (WDs) and vertically integrated water vapour transport (IVT) during February, March, and April (FMA) is illustrated in Figure 3(a, b). The climatology of WD intensity shows high values over the

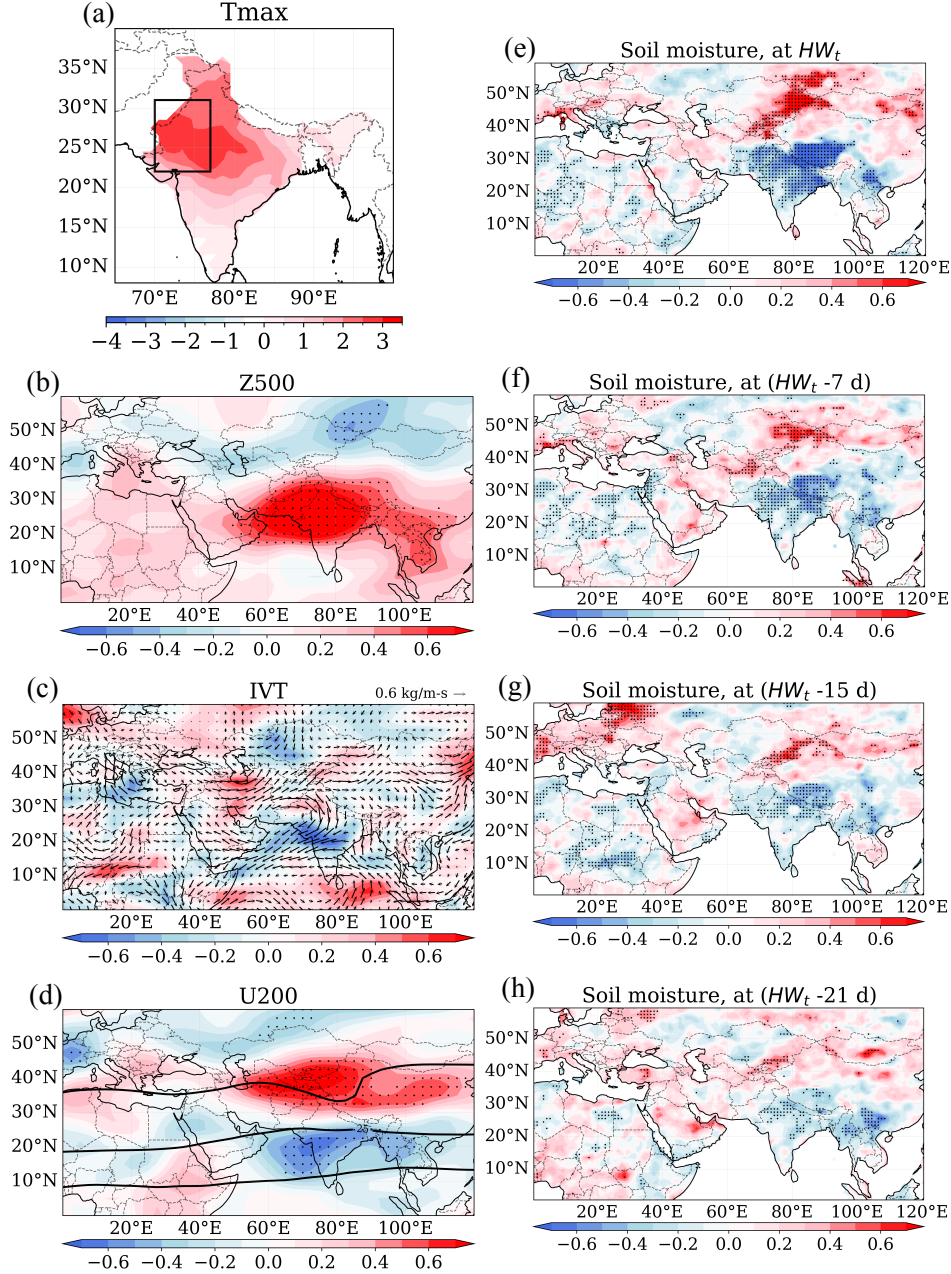


Figure 2: Composites of different climate variables linked to HWs in the NCI. (a) maximum temperature [$^{\circ}C$], (b) 500 hPa geopotential height [m], (c) integrated moisture transport (IVT) [$kgm^{-1}s^{-1}$], and (d) zonal wind at 200 hPa (U_{200}) [m/s] with black contours representing April-May climatology. Panels (e)-(h) depict soil moisture [m^3/m^3] anomalies occurring days to weeks before HWs, as indicated by the titles. Dotted areas highlight anomalies significant at the 95% level.

Mediterranean Sea, Iraq, Iran, Pakistan, and the northwest of India (Figure 3a). These intense WDs transport moisture from the Mediterranean, Red Sea, Persian Gulf, and northern Arabian Sea to northwest of India and the Himalayan region, continuing further east as shown in Figure 3b (Baudouin et al., 2021). The variability in moisture

transport over northern India is often associated with fluctuations in the intensity and frequency of WDs (Hunt et al., 2024).

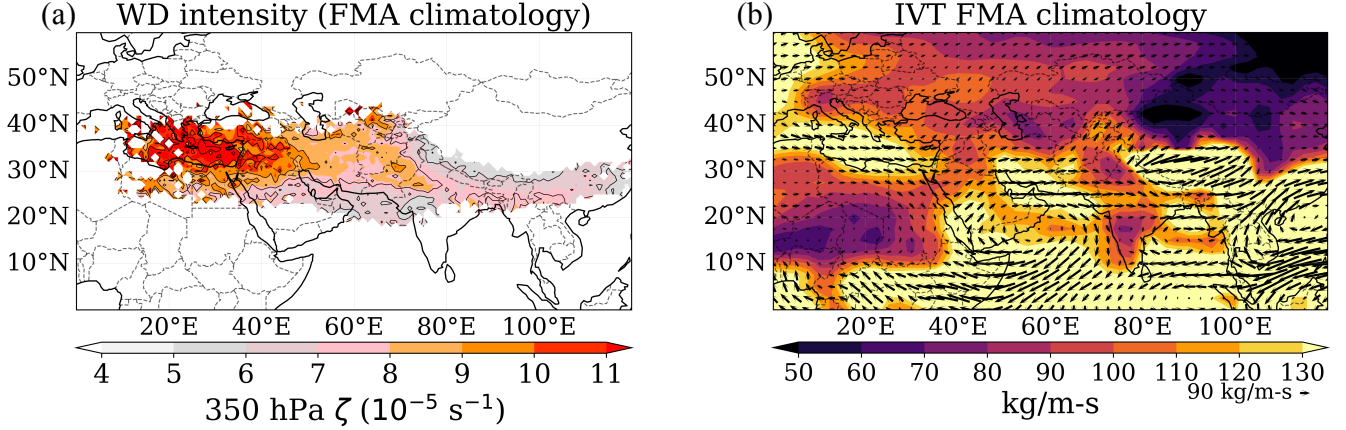


Figure 3: (a) February–April (FMA) climatology of the western disturbances (WDs) (350 hPa relative vorticity) derived from catalogue provided by Hunt and Zaz (2023). (b) Climatology of the vertically integrated moisture flux during same period.

Previous studies have reported that the position and intensity of the subtropical westerly jet (SWJ) influence WDs activity (Filippi et al., 2014; Dimri et al., 2015; Hunt and Zaz, 2023; Hunt et al., 2018b). The position of the SWJ influences the baroclinic interaction between WDs and the low-level moisture flow from the Arabian Sea (Hunt et al., 2024). Hunt and Zaz (2023) found that a northward shift in the SWJ position causes a poleward shift in WDs activity. Such a poleward shift in the SWJ has been previously linked using paleoclimatic records with hot and dry spring in the north-western Himalaya region (Thapa et al., 2020). The variability of the SWJ is closely related to the climate conditions over its North Atlantic entry point to Eurasia (Hunt and Zaz, 2023).

Here we use EOF analysis of U_{200} anomaly during FMA in the North Atlantic to investigate the relationship between the jet position and the dynamics of moisture flow which are associated with anomalously low soil moisture conditions over northern India.

The first EOF (EOF1) of the U_{200} anomaly during FMA in the North Atlantic region, shown in Figure 4a, explains 19% of the variance. The principal component time series (PC1) associated with EOF1 positively correlates with the jet position and waviness. High positive values of the PC1 are found to be related to the northward shift of the jet (Hunt and Zaz, 2023). Then, we use the PC1 time series and construct P_{jet} index which computes the time indices when PC1 is persistently high for 7 days above a threshold (here it is 90% of the PC1). The U_{200} anomaly associated with the P_{jet} indices indicates a northward movement in U_{200} (Figure 4b). In Figure 4b, green dots denote the climatology of the SWJ and yellow dots indicate the SWJ associated with P_{jet} indices.

The moisture flow (IVT) associated with the P_{jet} indices shows an increased influx of moisture from the Mediterranean Sea, Black Sea and Caspian Sea to the northwest part of Iran, parts of Afghanistan, Tajikistan and the western Himalayan region (Figure 4d). In contrast, low moisture flow is observed over northwestern India (Figure 4d), compared to the climatology (Figure 3b). We see a reduced moisture flow in the southern parts of Iran, which may be linked to a decrease WD activity in this region (Figure 4c). Furthermore, the influx of moisture from the north of the Arabian Sea to southern Pakistan and northwest India is reduced during the presence of persistent jet conditions. The P_{jet} indices can therefore identify the times when the connection between upper-level synoptic-scale disturbances and low-level moisture transport from the Arabian subtropical gyre weakens, providing valuable insights into moisture flow dynamics in the region.

Using the P_{jet} indices we can study the impact of the change in moisture dynamics associated with persistent jet conditions on soil moisture variability over India. Soil moisture anomalies over northern India exhibit a lagged response to U_{200} in the Atlantic region (Figure A2). Specifically, positive U_{200} anomalies in the North Atlantic

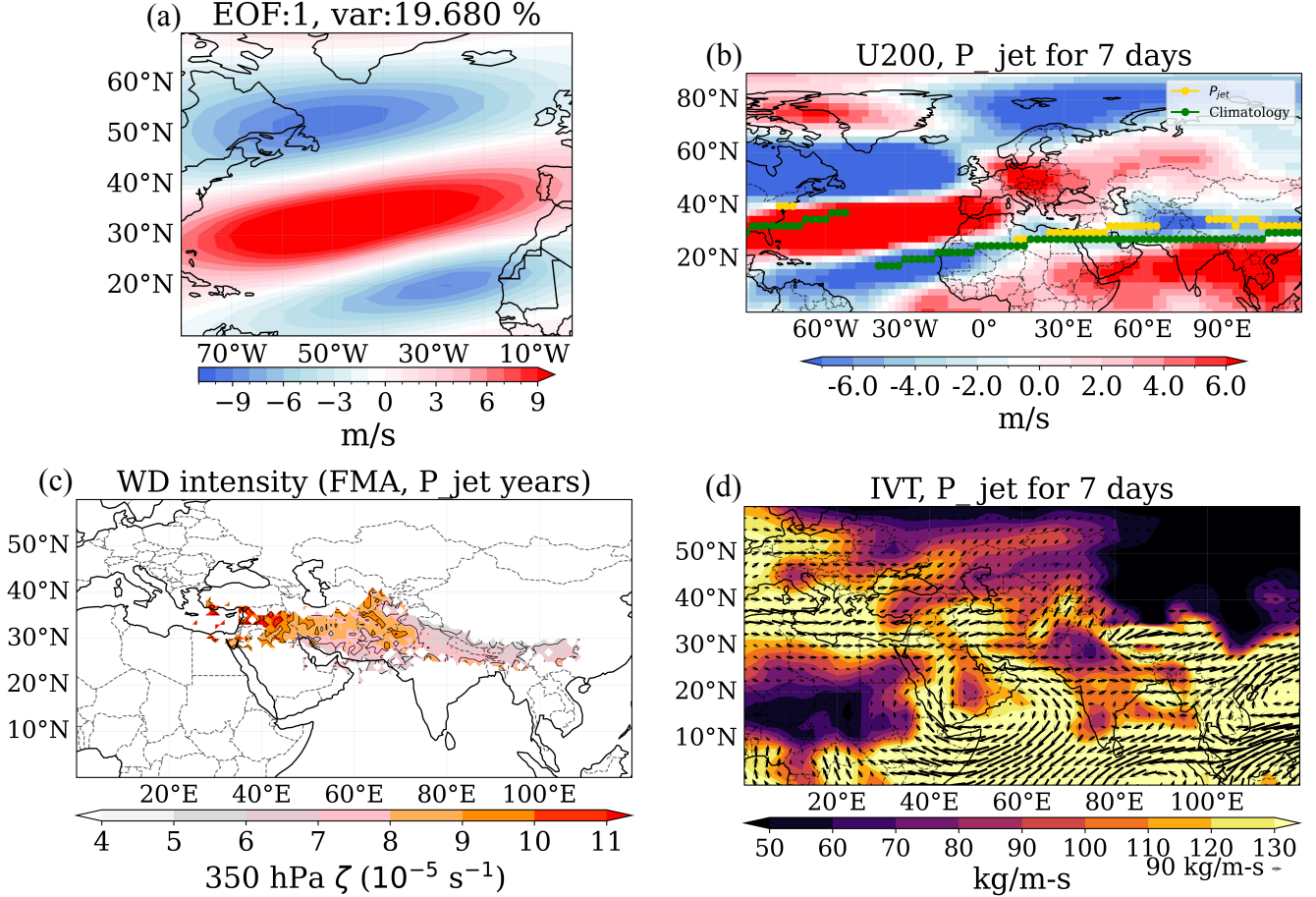


Figure 4: (a) EOF 1 of the U_{200} anomaly during February-March-April (FMA). (b) U_{200} anomaly associated with the 90th percentile of PC1 persists for 7 days. Green dots indicate the climatology of the SWJ, and yellow dots denote the SWJ associated with P_{jet} indices. The position of the SWJ is computed by taking a meridional local maximum in 200 hPa wind speed (U) where U exceeds 30 m/s (Hunt and Zaz, 2023). (c) Mean WDs during FMA for P_{jet} years. (d) Moisture flux (IVT) associated with P_{jet} indices.

during February–March is positively correlated with negative soil moisture conditions over northern India during April–May. We also find that the soil moisture negative response to the P_{jet} is lowest at 20 days after the occurrence of P_{jet} (vertical red line in Figure 5b). Figure 5a shows the composites of anomalous soil moisture fields associated with 20 days after the occurrence of P_{jet} . A significantly negative soil moisture anomaly can be observed over northern India.

Identification of the occurrence of the persistent jet using EOF-based analysis of zonal wind over the North Atlantic provides crucial insights into moisture flow dynamics and subsequent soil moisture variability. P_{jet} indices enable us to distinguish the favourable atmospheric circulation patterns that influence local climate conditions typical for HW occurrence over India (Table 1). Approximately 84.62% of the P_{jet} events occurred during a heat wave (HW) year. Furthermore, 53.85% of the P_{jet} events occurred during a HW in the northwestern part. When considering the total number of recorded HW years, the percentage of P_{jet} events during a HW in the northwestern part is approximately 33.33% (see Tables 4.2 and 4.3 in Rajeevan et al. (2023)). Rousi et al. (2022) associated an increase in the frequency and persistence of double jet stream states over Eurasia with occurrence of western Europe HWs.

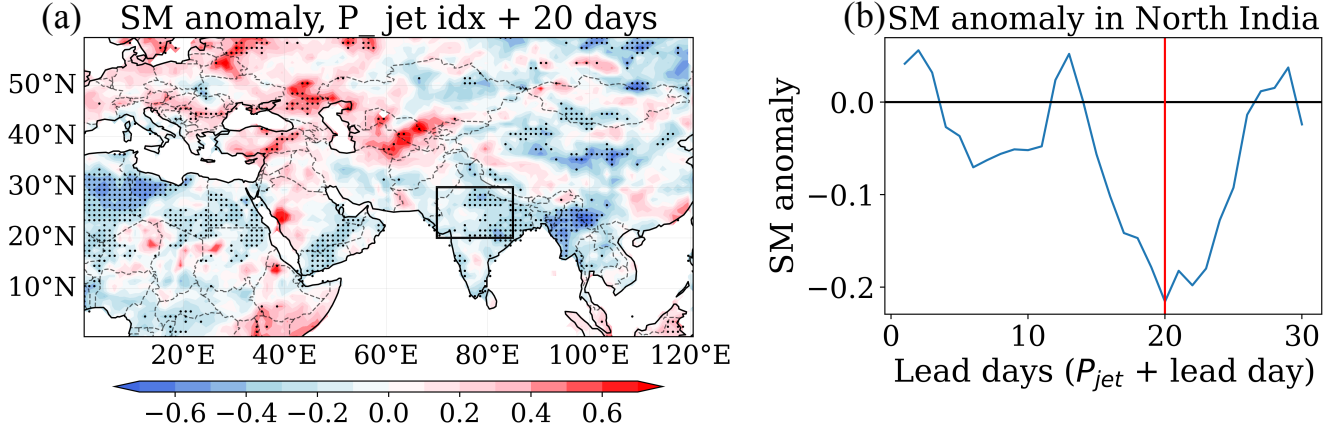


Figure 5: (a) Soil moisture anomaly [m^3/m^3] 20 days (vertical red line in (b)) after the occurrence of P_{jet} . (b) SM anomaly [m^3/m^3] over the North India (black box in (a)) for different lead times, red vertical line denotes the 20 day after the occurrence of P_{jet}

However, it should be noted that the identification of P_{jet} indices, based on a 7-day persistent high value of PC1 and its response to low soil moisture in India within the selected time window of 20 days, is empirically derived.

Table 1: List of P_{jet} indices year, frequency, HWs

P_{jet} occurrence	Frequency	Heat wave onset	Areas affected
1980-02-01, 1980-02-08	2	18 April	Northwest India
1981-03-04, 1981-03-11, 1981-03-18	3	15 Jun	Northwest India
1985-02-05	1	23 April, 1st May	East coast of India
1987-02-13	1	7 April	East coast of India
1988-04-11	1	10 April, 8 May, 26 May	Northwest India
1995-02-01	1	30 May	Northwest India
1997-04-16	1	29 May	East coast of India
2005-03-09	1	19 June	Northwest India
2006-03-22	1	-	None reported
2007-02-05, 2007-02-16	2	15 May	East coast of India
2010-02-03, 2010-02-10, 2010-02-17, 2010-03-03	4	8 April, 19 May, 19 June; 1 April, 9 April	Northwest India, East coast
2013-03-02, 2013-03-23	2	18 May	Northwest India
2018-03-02, 2018-03-09	2	-	None reported

In summary, the observational study using reanalysis data highlights the role of local soil moisture in the development of heat wave conditions in the NCI region. It suggests that these extreme heat events during April-May are driven not only by local weather patterns on a weekly scale but also by a complex interplay of large-scale factors, such as the persistence of jet stream states, which operate over monthly timescales. Therefore, it is crucial to investigate whether these factors have a causal impact on the occurrence of extreme temperatures in northern India. In the following section, we utilize an adjoint-based approach and perturbation experiments to explore the sensitivity of extreme temperatures to these factors.

4 Revealing causal drivers of NCI Heatwave: Model-based study

4.1 Adjoint sensitivity analysis

Adjoint sensitivities can identify local and remote influences of model parameters on the cost function specified as the area-averaged $T2m$ over northern India (Figure 1 and eq.1). Figure 6 displays the ensemble-mean adjoint sensitivity

of $T2m$ averaged over the masked region with respect to a few model parameters, going backward in time from t_0 to $t_0 - 6$ days, where t_0 is the HW onset date.

The sensitivity to ocean surface temperature (SST) can be identified over the specified time frame to originate mainly from the Arabian Sea (Figures 6(a - c)). The figure reveals that the $T2m$ sensitivity to SST is very small at day 0, but grows as we go back in time and it can be anticipated that it amplifies further with increasing lead times. Positive SST sensitivity originates in the north east of the Arabian Sea expanding up to the North of the Indian Ocean and south west of the Bay of Bengal for day -3 to -6. Positive sensitivity implies that the temperature increment in the masked region is associated with positive fluctuation in the SST over this region. Previous studies have also reported a significant positive influence of SST over the Arabian Sea and the western Indian Ocean on the temperature in northwestern India (Rohini et al., 2016; Dubey et al., 2021).

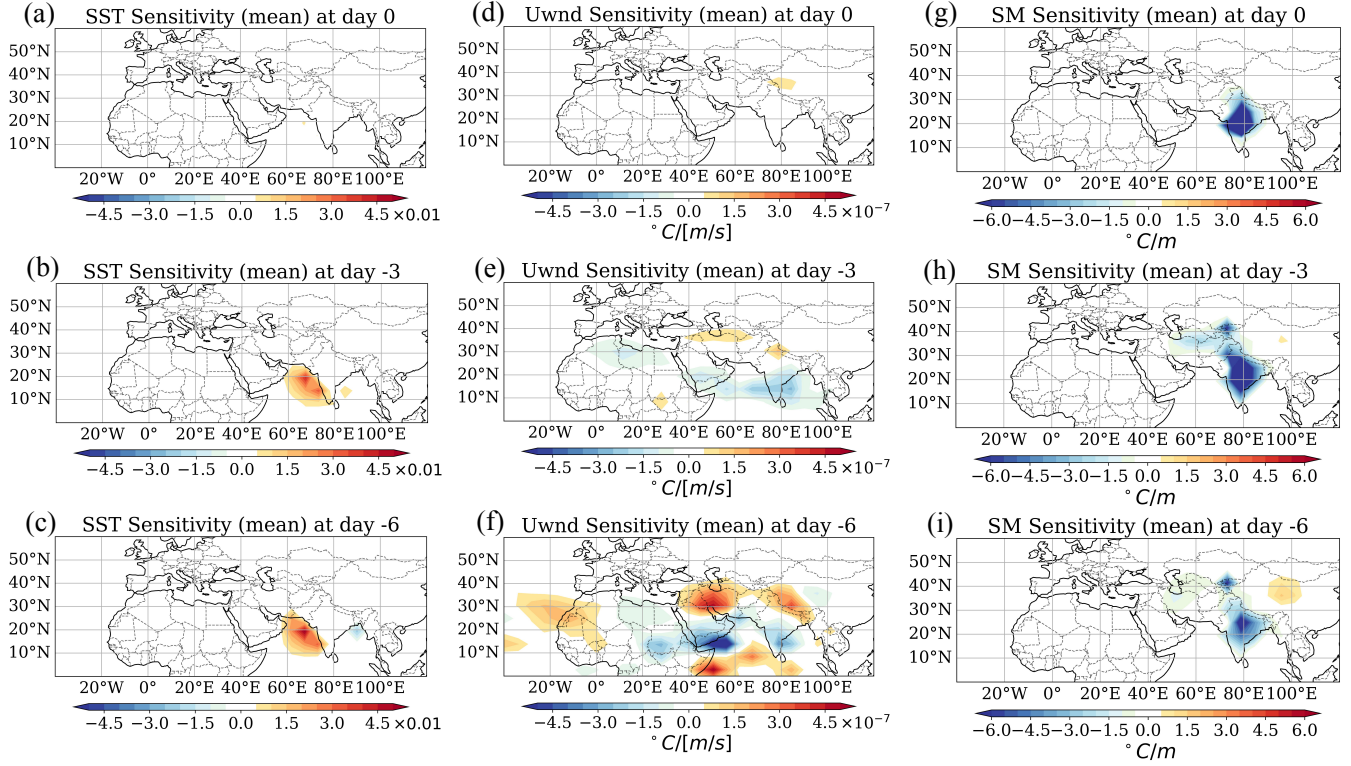


Figure 6: Adjoint sensitivities of the cost function eq. (1) plotted backward in time from day 0 in the top row to -6 days in the bottom row. The left column (a - c) shows sensitivities with respect to for SST. The middle column (d - f) shows the sensitivities with respect to the upper tropospheric zonal wind (model level 2 analogous to 200-250 hPa). The right column (g - i) shows the sensitivities with respect to soil moisture.

With respect to upper tropospheric zonal wind, we observe small positive sensitivity to wind anomalies over the western Tibetan Plateau, some part of the north India, northern Pakistan on the day of HW onset (day 0) as shown in Figure 6d. By day -3 (Figure 6e), the positive sensitivity over northern India expands, while the negative sensitivity begins to extend from central India towards Oman, Yemen and northern Africa. Upon integrating further backward (day -6), the negative sensitivity expands further west, and positive sensitivity is observed over the Atlantic towards the Atlantic entry point of the African jet, with additional low negative sensitivity observed over the west coast of India. Meanwhile, positive sensitivity stretches further eastward and westward from the Himalayan region. Notably, positive sensitivity is seen over Iran, Mediterranean regions. An increasing positive sensitivity is also observed over the western Indian Ocean region (Figure 6f). These sensitivity patterns (Figures 6d-f) show a resemblance with the $U200$ composite shown in Figure 2d. The positive sensitivity over northern India indicates that zonal wind over this

region is positively associated with the HW development in the north-central India. This can be linked with the shift in the zonal wind, as observed in Figure 2d and 3b. Despite the limitation in extending the analysis further backwards in time due to instability in the adjoint model, the upper tropospheric zonal wind sensitivity clearly indicates a robust link with remote large-scale circulation originating from the North Atlantic, thereby supporting our findings on the role of wind patterns associated with HWs as explained above.

A strong negative sensitivity of $T2m$ to the soil moisture (SM) can be seen over central India on the day of HW onset (Figure 6g). This negative sensitivity pattern indicates that dry local soil moisture strongly influences the HW development in this region which maintains our inference from the SM in the previous section (Figure 2h). As we integrate backward in time, negative sensitivity weakens and also spreads to the north of India, northern Pakistan, and southwestern Tibetan Plateau (Figures 6h,i). It is evident from both the observation and the adjoint-based sensitivity study, persistent low soil moisture is an important pre-requisite for the development of HWs. However, the biggest impact of SM on $T2m$ appears to come 1 day prior to the onset of heat wave; prior to this soil moisture could be more important to reshape the atmospheric flow via land-atmospheric feedback processes. It must be noted that the relative importance of the individual sensitivities (Figure 6) of the cost function can only be inferred qualitatively in this case as it requires the knowledge of expected anomalies to quantify their impact. We will analyse the individual contributions to a HW in the following step.

From the adjoint sensitivity analysis above, we see that soil moisture has a localized dominant and robust affect on $T2m$ few days before the HW event. It is therefore of interest to quantify the relative contribution of SM to the temperature anomaly during a HW event. The response function of the linear adjoint model to SM can be evaluated by computing the dot product between the anomaly (here, the deseasonalized and detrended SM anomaly from the reanalysis data) and the sensitivity field, e.g., SM sensitivity ($\frac{\delta T_{2m}}{\delta SM}$) (Köhl and Vlasenko, 2019). The response function is computed as follows:

$$\text{Response}\% = 100 \times \frac{\left(\frac{\delta T_{2m}}{\delta SM} \Big|_{t'} \right) \cdot SM_{\text{anomaly}}(HW_t - t')}{\max_{HW_t \leq t \leq HW_t + 10} T_{2m, \text{anomaly}}(t) \Big|_{\text{NCI}}}$$

where t' denotes the day of minimum sensitivity for soil moisture, SM_{anomaly} is the observational soil moisture anomaly, HW_t is the onset of the HWs provided by the IMD (Section 2), and $T_{2m, \text{anomaly}}$ is the temperature anomaly at NCI (Figure 2a). We consider the maximum temperature anomaly between the onset and 10 days after the onset of the HW for the response function.

For the soil moisture sensitivity field, we find that the minimum sensitivity occurs at $t' = -1$. Figure 7(a) shows that the mean contribution of soil moisture to the temperature anomaly during all heatwaves in NCI is approximately 32%. Additionally, we examine the SST response function and find that the maximum sensitivity for SST occurs at $t' = -6$, as shown in Figure 7(b). We also investigate the contribution of upper-tropospheric zonal wind, but the responses are very small.

4.2 Forward perturbation runs

As the adjoint cannot be run backwards for longer than 1 week because of the fast growing nonlinear modes, it is difficult to infer the sensitivities of soil moisture over NCI stemming from regions further remote. However, we can demonstrate these dependencies in forward perturbation runs.

In Section 3, we observed that the variability of the SWJ during FMA is associated with hot and dry conditions over India during April–May. The adjoint sensitivity analysis also revealed a strong connection to the SWJ (Figures 6e,f). Several studies have associated changes in the sea surface temperature (SST) of the tropical Atlantic to a strengthening of the subtropical jet to the north (Brayshaw et al., 2009). In agreement with these studies, we also observed a positive SST anomaly in the North Atlantic region during the occurrence of the P_{jet} (Figure A3). It is therefore intriguing to investigate whether the North Atlantic SST plays indeed a role in moderating the large-scale circulations and whether these changes lead to dry soil conditions thereby exacerbating high temperatures over India.

To investigate this question, we added a positive anomaly to the initial state to the North Atlantic SST in PlaSim’s. We introduce this anomaly by creating a weighted mask (Figure 8), which is then added to the initial SST

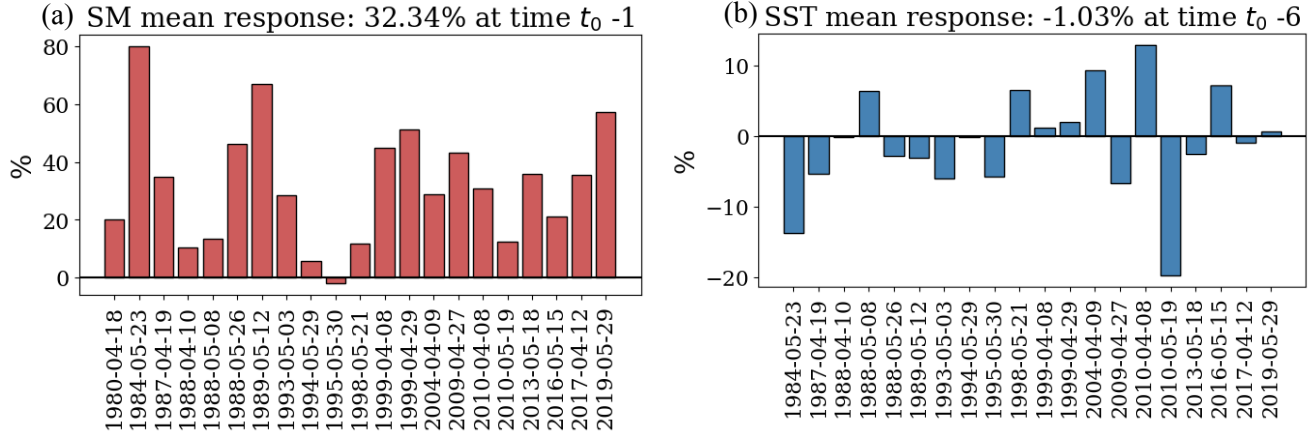


Figure 7: (a) Soil moisture contribution to the temperature anomaly for different HW (-5 to 0 days, where Day 0 is the HW onset) events is shown

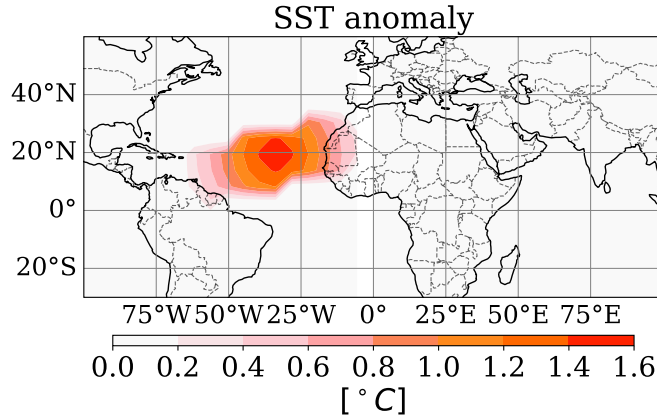


Figure 8: SST perturbation mask for forward runs.

values in the North Atlantic Ocean separately for February and March. Thereafter, we run the model forward up to the month of May. PlaSim has a slab ocean model of mixed layer depth of 50 meter. We repeat this experiment for 20 different starting years with similar perturbation adding to their initial values (20 ensemble members). Since we are investigating the heatwaves occurring in April-May, we calculate the mean difference of various variables between the perturbed and unperturbed SST conditions during this period. The motivation behind perturbing the SST of the North Atlantic during this time is drawn from our results presented in Section 3, where we were able to link the occurrence of persistent jet in Feb-Mar to the occurrence of HW events in Apr-May over India (Table 1).

The ensemble mean difference between normal atmospheric state and the conditions on perturbing north Atlantic SST (Feb/Mar) during April-May (AM) is shown in Figures 9 and 10. These figures demonstrate change in geopotential height at 500 hPa (Z500), upper tropospheric zonal wind at 200 hPa (U200), 2m air temperature (T2m), and soil moisture (SM). Upon perturbing SST during both February (Figure 9a) and March (Figure 10a) we observe a high pressure anomaly over the southeast of Iran, Pakistan, northern India, northwest of Europe, and low pressure over the Eurasian region. Z500 patterns exhibit a quasi-stationary Rossby wave pattern. These findings corroborate with (Ratnam et al., 2016) who also reported a causal relationship between high pressure system over northwestern Europe and India and a quasi-stationary Rossby wave pattern during HWs in NCI region.

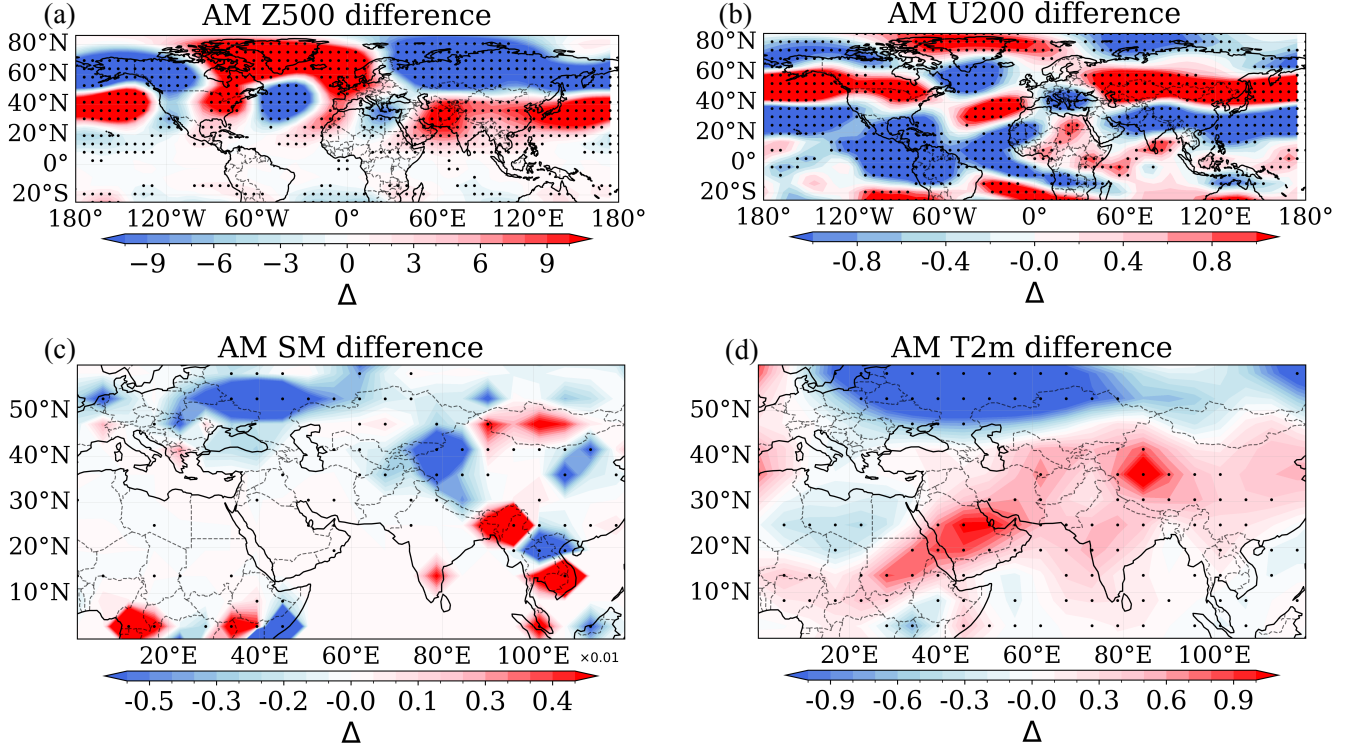


Figure 9: Ensemble mean difference for different variables during April and May (AM) for forward run experiments in which the North Atlantic SST was perturbed (as shown in Figure 8) in the beginning of February: (a) Z500 [m], (b) U200 [m/s], (c) soil moisture [m], (d) 2m air temperature [°C]. Black dots denote 95% significance.

The highest zonal wind anomaly can be seen over the Eurasian region (mainly over Kazakhstan, Kyrgyzstan, Uzbekistan) for both the February (Figure 9b) and the March (Figure 10b) perturbation. We also observe significant negative anomaly over central India. These patterns bear close resemblance with the northward shift U200 pattern associated with HWs in NCI shown in Figure 2d. We also observe a significant negative soil moisture anomaly stretching over Tibetan Plateau, Himalayan region (Figures 9c and 10c). This pattern has similarity with the SM conditions prior and during HW events (Figures 2e,f,g,h) and those ≈ 3 weeks after P_{jet} (Figures 5a). On the other hand, a positive soil moisture anomaly pattern is seen over northern Pakistan extending north eastwards to Kazakhstan, Russia and Mongolia, which may be related to changed moisture dynamics associated with the northward shift of SWJ in previous months as reported in Section 3 (Figure 4d). This dipole-like pattern in SM anomaly is similar to that observed from reanalysis data weeks before and during HW events (Figures 2e,f,g and h). The disparity between the intensity of negative SM anomaly over Indo-Gangetic plain and Himalayan belt, and the rest of India, in particular, a very weak signal of drier than normal SM conditions on perturbation of Atlantic SST might be partly associated with the fact that here we compute the mean SM conditions over a span of two months and partly due to model limitations. The latter includes coarse grid resolution, and generally weak moisture dynamics and precipitation biases.

Finally, Figures 9d and 10d show an overall significant positive anomaly of T2m over India in both cases of perturbation. The higher temperature anomaly observed in the northeastern parts of India, compared to the rest of the country, can be attributed to factors similar to those previously discussed in relation to the negative soil moisture (SM) anomaly. It is important to note that despite the limitations of our simulations, such as the intermediate complexity of the model and the coarse resolution, our findings are consistent with those from our observational

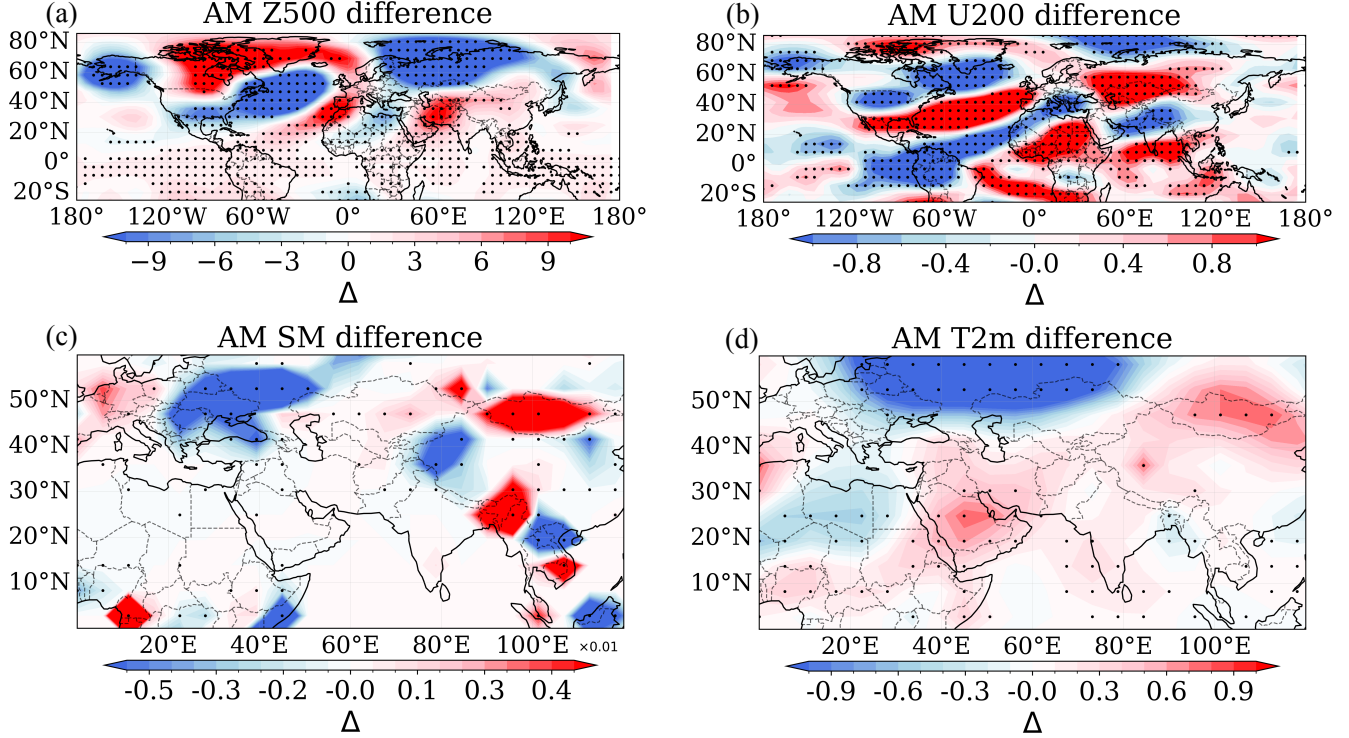


Figure 10: Ensemble mean difference for different variables during April and May (AM) for forward run experiments in which the North Atlantic SST was perturbed (as shown in Figure 8) in the beginning of March: (a) Z500 [m], (b) U200 [m/s], (c) soil moisture [m], (d) 2m air temperature [$^{\circ}C$]. Black dots denote 95% significance.

study detailed in Section 3. Our forward experiments demonstrate the significant influence of North Atlantic Ocean sea surface temperatures (SST) on large-scale atmospheric circulation over India. Specifically, our findings reveal that the dynamical changes in the atmosphere, driven by SST variations during February and March, can lead to increased temperatures over India in April-May through modulation of the upper tropospheric winds.

5 Conclusion

In this paper we provide a new working hypothesis for the development and causes of heatwaves over north-central India during April–May based on a combined analysis of atmospheric reanalysis fields and adjoint model-based approaches. Through our reanalysis study, we identified potential mechanisms leading to heatwaves over northern India. In combination with our novel adjoint sensitivity approach and perturbation runs, we identify the possible causal influence of local and remote factors causing extreme heat conditions in India. Our results highlight a sequence of processes leading to heatwave development over this region begins to unfold months before the heatwaves actually occur.

The proposed mechanism of heatwave development over India is summarized as follows:

1. Anomalously high sea surface temperatures occurring over the North Atlantic during February and March influence the variability of the subtropical westerly jet leading to teleconnections that can modulate weather conditions over the Indian subcontinent.
2. Atmospheric dynamical changes in the North Atlantic lead to a northward shift in the position of the subtropical jet. Perturbation forward experiments show that anomalous SST within specific regions of the North

Atlantic lead to changes in large-scale atmospheric patterns over monthly timescales, resulting in increased temperatures over northern India. The intensity and spatial extents of the SST anomalies applied in this study were empirically determined.

3. This altered state of the subtropical jet can persist over several days which affects the area and intensity of the western disturbances embedded in it.
4. Change in the upper tropospheric conditions reduces winter–spring moisture flow to the northern India. As western disturbances generally bring moisture in the Middle East and northwestern parts of India during boreal winter–spring, the altered upper tropospheric conditions influence the moisture dynamics in this region. This includes reduced moisture flow to northern India from the north of the Arabian Sea during winter–spring.
5. Reduced moisture flow affects local soil moisture variability creating conditions conducive for heatwave development. Adjoint sensitivity analysis indicated that dry soil moisture prior to the onset of heatwaves strongly influences heatwave development, even though the backward integration was limited up to 6 days due to non-linear instability of the adjoint model. Moreover, significant reduction in soil moisture was observed from reanalysis study weeks before the onset of April–May heatwaves in India.
6. Persistent low moisture before a heatwave can act as a preconditioning factor, establishing ideal conditions for heatwaves development. Consequently, extreme heat conditions occur during April–May over north-central India.

Identifying the preconditioning factors that lead to heatwave development is crucial for making accurate sub-seasonal predictions. In this context, it would be highly valuable to assess and evaluate the effectiveness of these factors in predicting heatwaves using high-resolution Earth system models and machine learning techniques. Further research is needed to explore the effects of varying the intensities and spatial extents of the SST in the North Atlantic to fully understand their impact on heatwaves over India. A rigorous analysis is also required to fully uncover the relationship between P_{jet} and soil moisture variability over India, which is beyond the scope of this study.

Acknowledgement

This research was supported, in part, through the Koselleck grant Earth^{RA} from the Deutsche Forschungsgemeinschaft. Contribution to the Centrum für Erdsystemforschung und Nachhaltigkeit (CEN) of Universität Hamburg.

Data

We utilize daily maximum temperature data over India from 1980 to 2022, as provided by the India Meteorological Department (Srivastava et al., 2009). For atmospheric variables, we use daily data from the NCEP-NCAR Reanalysis 1 for the same time period (Kalnay et al., 2018). Daily surface soil moisture data is sourced from GLEAM v3.8a (Martens et al., 2017). Precipitation data is obtained from the GPCC monthly precipitation product (Schneider et al., 2016)⁴. Additionally, we use the NOAA Optimum Interpolation (OI) sea surface temperature (SST) V2 high-resolution daily data from 1982 to 2022 (Huang et al., 2021), regridded to the PlaSim grid for SST response function analysis, and the NOAA Extended Reconstructed SST (V5) monthly data for composite analysis (Huang et al., 2017).

Appendix

We identify the heatwave years and compute the composites of standardize precipitation anomaly for April-May and also the months before.

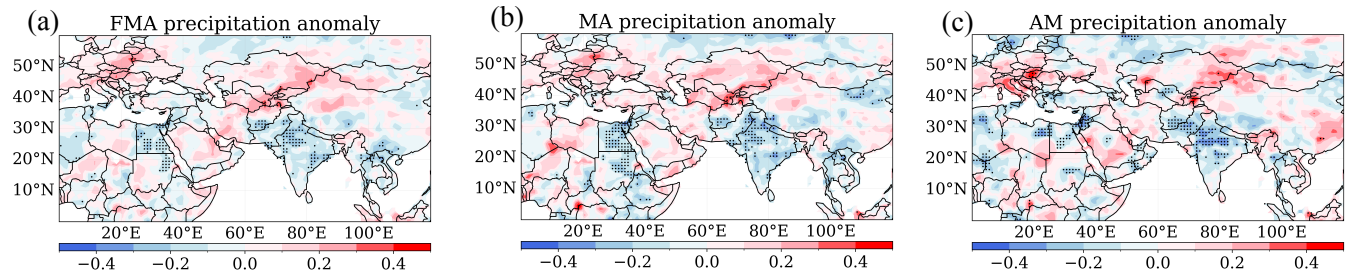


Figure A1: GPCC monthly precipitation [$mm/month$] anomaly on HW years, (a) February-April, (b) March-April, (c) April-May

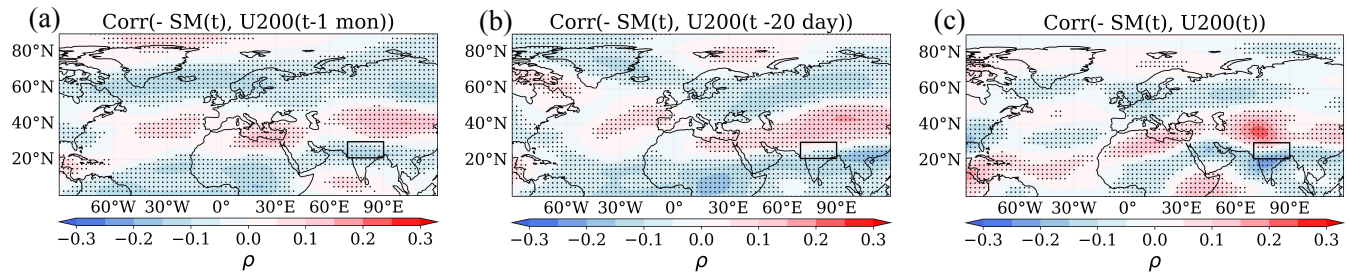
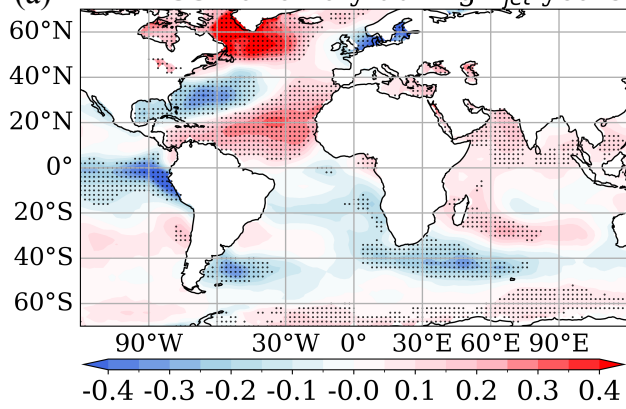


Figure A2: April-May Correlation between Soil moisture anomaly over north India and $U200$ with lags, ρ denotes the correlation strength, black dots imply 95% significance.

We compute the SST anomaly using the long term climatology between 1991-2020 provided by <https://downloads.psl.noaa.gov/Datasets/noaa.ersst.v5/>

⁴https://opendata.dwd.de/climate_environment/GPCC/html/fulldata-monthly_v2022_doi_download.html

(a) FMA SST anomaly during P_{jet} years



(b) FMA SST anomaly during HW years

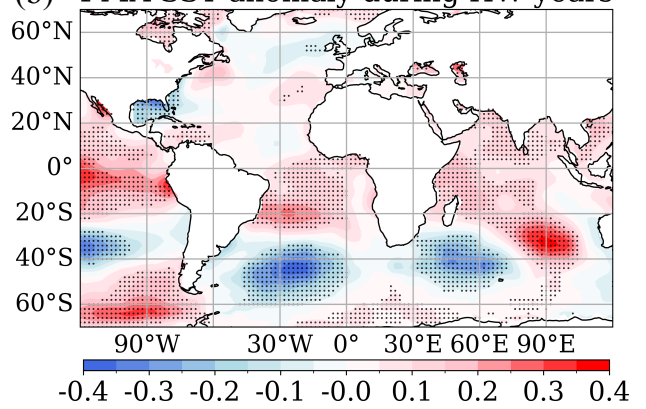


Figure A3: Monthly sea surface temperature anomaly [$^{\circ}C$] during February-March-April (FMA) for (a) P_{jet} years, (b) HW years. Black dots imply 95% significance.

References

- Alexander, L. (2011). Extreme heat rooted in dry soils. *Nature Geoscience*, 4(1):12–13.
- Barriopedro, D., García-Herrera, R., Ordóñez, C., Miralles, D., and Salcedo-Sanz, S. (2023). Heat waves: Physical understanding and scientific challenges. *Reviews of Geophysics*, page e2022RG000780.
- Baudouin, J.-P., Herzog, M., and Petrie, C. A. (2021). Synoptic processes of winter precipitation in the Upper Indus Basin. *Weather and Climate Dynamics*, 2(4):1187–1207.
- Berg, A., Lintner, B. R., Findell, K., Seneviratne, S. I., van Den Hurk, B., Ducharne, A., Chéruy, F., Hagemann, S., Lawrence, D. M., Malyshev, S., et al. (2015). Interannual coupling between summertime surface temperature and precipitation over land: Processes and implications for climate change. *Journal of Climate*, 28(3):1308–1328.
- Blessing, S., Kaminski, T., Lunkeit, F., Matei, I., Giering, R., Köhl, A., Scholze, M., Herrmann, P., Fraedrich, K., and Stammer, D. (2014). Testing variational estimation of process parameters and initial conditions of an earth system model. *Tellus A: Dynamic Meteorology and Oceanography*, 66(1):22606.
- Brayshaw, D. J., Woollings, T., and Vellinga, M. (2009). Tropical and extratropical responses of the North Atlantic atmospheric circulation to a sustained weakening of the MOC. *Journal of Climate*, 22(11):3146–3155.
- Campbell, S., Remenyi, T. A., White, C. J., and Johnston, F. H. (2018). Heatwave and health impact research: A global review. *Health & place*, 53:210–218.
- Dawson, A. (2016). eofs: A library for eof analysis of meteorological, oceanographic, and climate data.
- de Bont, J., Nori-Sarma, A., Stafoggia, M., Banerjee, T., Ingole, V., Jaganathan, S., Mandal, S., Rajiva, A., Krishna, B., Kloog, I., et al. (2024). Impact of heatwaves on all-cause mortality in India: A comprehensive multi-city study. *Environment international*, 184:108461.
- Debnath, R., Bardhan, R., and Bell, M. L. (2023). Lethal heatwaves are challenging India’s sustainable development. *PLOS climate*, 2(4):e0000156.
- Dimri, A., Niyogi, D., Barros, A., Ridley, J., Mohanty, U., Yasunari, T., and Sikka, D. (2015). Western disturbances: a review. *Reviews of Geophysics*, 53(2):225–246.
- Domeisen, D. I., Eltahir, E. A., Fischer, E. M., Knutti, R., Perkins-Kirkpatrick, S. E., Schär, C., Seneviratne, S. I., Weisheimer, A., and Wernli, H. (2023). Prediction and projection of heatwaves. *Nature Reviews Earth & Environment*, 4(1):36–50.
- Dubey, A. K., Kumar, P., Saharwardi, M. S., and Javed, A. (2021). Understanding the hot season dynamics and variability across India. *Weather and Climate Extremes*, 32:100317.
- Filippi, L., Palazzi, E., von Hardenberg, J., and Provenzale, A. (2014). Multidecadal variations in the relationship between the NAO and winter precipitation in the Hindu Kush–Karakoram. *Journal of climate*, 27(20):7890–7902.
- Fischer, E. M., Seneviratne, S. I., Lüthi, D., and Schär, C. (2007a). Contribution of land-atmosphere coupling to recent European summer heat waves. *Geophysical Research Letters*, 34(6).
- Fischer, E. M., Seneviratne, S. I., Vidale, P. L., Lüthi, D., and Schär, C. (2007b). Soil moisture–atmosphere interactions during the 2003 European summer heat wave. *Journal of Climate*, 20(20):5081–5099.
- Fraedrich, K., Jansen, H., Kirk, E., Luksch, U., and Lunkeit, F. (2005). The Planet Simulator: Towards a user friendly model. *Meteorologische Zeitschrift*, 14(3):299–304.
- Ganeshi, N. G., Mujumdar, M., Krishnan, R., and Goswami, M. (2020). Understanding the linkage between soil moisture variability and temperature extremes over the Indian region. *Journal of Hydrology*, 589:125183.

- Ganeshi, N. G., Mujumdar, M., Takaya, Y., Goswami, M. M., Singh, B. B., Krishnan, R., and Terao, T. (2023). Soil moisture revamps the temperature extremes in a warming climate over India. *npj Climate and Atmospheric Science*, 6(1):12.
- García-León, D., Casanueva, A., Standardi, G., Burgstall, A., Flouris, A. D., and Nybo, L. (2021). Current and projected regional economic impacts of heatwaves in Europe. *Nature communications*, 12(1):5807.
- Hari, V., Ghosh, S., Zhang, W., and Kumar, R. (2022). Strong influence of north Pacific Ocean variability on Indian summer heatwaves. *Nature communications*, 13(1):5349.
- Horton, D. E., Johnson, N. C., Singh, D., Swain, D. L., Rajaratnam, B., and Diffenbaugh, N. S. (2015). Contribution of changes in atmospheric circulation patterns to extreme temperature trends. *Nature*, 522(7557):465–469.
- Horton, R. M., Mankin, J. S., Lesk, C., Coffel, E., and Raymond, C. (2016). A review of recent advances in research on extreme heat events. *Current Climate Change Reports*, 2:242–259.
- Huang, B., Liu, C., Banzon, V., Freeman, E., Graham, G., Hankins, B., Smith, T., and Zhang, H.-M. (2021). Improvements of the daily optimum interpolation sea surface temperature (DOISST) version 2.1. *Journal of Climate*, 34(8):2923–2939.
- Huang, B., Thorne, P. W., Banzon, V. F., Boyer, T., Chepurin, G., Lawrimore, J. H., Menne, M. J., Smith, T. M., Vose, R. S., Zhang, H.-M., et al. (2017). NOAA extended reconstructed sea surface temperature (ERSST), version 5. *NOAA National Centers for Environmental Information*, 30(8179-8205):25.
- Hunt, K. M. (2024). Increasing frequency and lengthening season of western disturbances are linked to increasing strength and delayed northward migration of the subtropical jet. *Weather and Climate Dynamics*, 5(1):345–356.
- Hunt, K. M., Baudouin, J.-P., Turner, A. G., Dimri, A., Jeelani, G., Pooja, Chattopadhyay, R., Cannon, F., Arulalan, T., Shekhar, M., et al. (2024). Western disturbances and climate variability: a review of recent developments. *EGU sphere*, 2024:1–106.
- Hunt, K. M., Turner, A. G., and Shaffrey, L. C. (2018a). Extreme daily rainfall in Pakistan and north India: Scale interactions, mechanisms, and precursors. *Monthly Weather Review*, 146(4):1005–1022.
- Hunt, K. M., Turner, A. G., and Shaffrey, L. C. (2018b). The evolution, seasonality and impacts of western disturbances. *Quarterly Journal of the Royal Meteorological Society*, 144(710):278–290.
- Hunt, K. M. and Zaz, S. N. (2023). Linking the North Atlantic Oscillation to winter precipitation over the Western Himalaya through disturbances of the subtropical jet. *Climate Dynamics*, 60(7):2389–2403.
- Im, E.-S., Pal, J. S., and Eltahir, E. A. (2017). Deadly heat waves projected in the densely populated agricultural regions of South Asia. *Science advances*, 3(8):e1603322.
- Jaeger, E. B. and Seneviratne, S. I. (2011). Impact of soil moisture–atmosphere coupling on European climate extremes and trends in a regional climate model. *Climate Dynamics*, 36(9):1919–1939.
- Joy, A. and Satheesan, K. (2022). Influence of soil moisture on mean daily maximum and minimum temperatures over India. *Meteorology and Atmospheric Physics*, 134(3):49.
- Kalnay, E., Kanamitsu, M., Kistler, R., Collins, W., Deaven, D., Gandin, L., Iredell, M., Saha, S., White, G., Woollen, J., et al. (2018). The NCEP/NCAR 40-year reanalysis project. In *Renewable energy*, pages Vol1_146–Vol1_194. Routledge.
- Köhl, A. and Vlasenko, A. (2019). Seasonal prediction of northern European winter air temperatures from SST anomalies based on sensitivity estimates. *Geophysical Research Letters*, 46(11):6109–6117.

- Koster, R. D., Chang, Y., Wang, H., and Schubert, S. D. (2016). Impacts of local soil moisture anomalies on the atmospheric circulation and on remote surface meteorological fields during boreal summer: A comprehensive analysis over North America. *Journal of Climate*, 29(20):7345–7364.
- Koster, R. D., Sud, Y., Guo, Z., Dirmeyer, P. A., Bonan, G., Oleson, K. W., Chan, E., Versegny, D., Cox, P., Davies, H., et al. (2006). GLACE: the global land–atmosphere coupling experiment. Part I: overview. *Journal of Hydrometeorology*, 7(4):590–610.
- Kumar, R., Kuttippurath, J., Gopikrishnan, G., Kumar, P., and Varikoden, H. (2023). Enhanced surface temperature over India during 1980–2020 and future projections: causal links of the drivers and trends. *npj Climate and Atmospheric Science*, 6(1):164.
- Lekshmi, S. and Chattopadhyay, R. (2022). Modes of summer temperature intraseasonal oscillations and heatwaves over the Indian region. *Environmental Research: Climate*, 1(2):025009.
- Lorenz, R., Jaeger, E. B., and Seneviratne, S. I. (2010). Persistence of heat waves and its link to soil moisture memory. *Geophysical Research Letters*, 37(9).
- Lyu, G., Köhl, A., Matei, I., and Stammer, D. (2018). Adjoint-based climate model tuning: Application to the planet simulator. *Journal of Advances in Modeling Earth Systems*, 10(1):207–222.
- Marotzke, J., Giering, R., Zhang, K. Q., Stammer, D., Hill, C., and Lee, T. (1999). Construction of the adjoint MIT ocean general circulation model and application to Atlantic heat transport sensitivity. *Journal of Geophysical Research: Oceans*, 104(C12):29529–29547.
- Martens, B., Miralles, D. G., Lievens, H., Van Der Schalie, R., De Jeu, R. A., Fernández-Prieto, D., Beck, H. E., Dorigo, W. A., and Verhoest, N. E. (2017). GLEAM v3: Satellite-based land evaporation and root-zone soil moisture. *Geoscientific Model Development*, 10(5):1903–1925.
- Mazdiyasn, O., AghaKouchak, A., Davis, S. J., Madadgar, S., Mehran, A., Ragno, E., Sadegh, M., Sengupta, A., Ghosh, S., Dhanya, C., et al. (2017). Increasing probability of mortality during Indian heat waves. *Science advances*, 3(6):e1700066.
- Miralles, D. G., Van Den Berg, M., Teuling, A., and De Jeu, R. (2012). Soil moisture-temperature coupling: A multiscale observational analysis. *Geophysical Research Letters*, 39(21).
- Nandi, S. and Patel, P. (2020). iamsaswata/imdlib: a Python library for IMD gridded data. *Zenodo*, Dec, 31.
- Pai, D. and Nair, S. (2022). Impact of El-Niño-Southern Oscillation (ENSO) on extreme temperature events over India. *MAUSAM*, 73(3):597–606.
- Pai, D., NAIR, S., and Ramanathan, A. (2013). Long term climatology and trends of heat waves over India during the recent 50 years (1961-2010). *Mausam*, 64(4):585–604.
- Panda, D. K., AghaKouchak, A., and Ambast, S. K. (2017). Increasing heat waves and warm spells in India, observed from a multiaspect framework. *Journal of Geophysical Research: Atmospheres*, 122(7):3837–3858.
- Perkins, S. E. (2015). A review on the scientific understanding of heatwaves—Their measurement, driving mechanisms, and changes at the global scale. *Atmospheric Research*, 164:242–267.
- Pfahl, S. and Wernli, H. (2012). Quantifying the relevance of atmospheric blocking for co-located temperature extremes in the Northern Hemisphere on (sub-) daily time scales. *Geophysical Research Letters*, 39(12).
- Rajeevan, M., Rohini, P., Nair, S. A., and Snehalata Tirkey, Tanmoy Goswami, N. K. (2023). Heat and cold waves in india processes and predictability. *Met Monograph, IMD*.

- Ratnam, J., Behera, S. K., Ratna, S. B., Rajeevan, M., and Yamagata, T. (2016). Anatomy of Indian heatwaves. *Scientific reports*, 6(1):24395.
- Rohini, P., Rajeevan, M., and Mukhopadhyay, P. (2019). Future projections of heat waves over India from CMIP5 models. *Climate dynamics*, 53:975–988.
- Rohini, P., Rajeevan, M., and Srivastava, A. (2016). On the variability and increasing trends of heat waves over India. *Scientific reports*, 6(1):1–9.
- Röthlisberger, M. and Papritz, L. (2023). Quantifying the physical processes leading to atmospheric hot extremes at a global scale. *Nature Geoscience*, 16(3):210–216.
- Rousi, E., Kornhuber, K., Beobide-Arsuaga, G., Luo, F., and Coumou, D. (2022). Accelerated western European heatwave trends linked to more-persistent double jets over Eurasia. *Nature communications*, 13(1):3851.
- Russo, S., Dosio, A., Graversen, R. G., Sillmann, J., Carrao, H., Dunbar, M. B., Singleton, A., Montagna, P., Barbola, P., and Vogt, J. V. (2014). Magnitude of extreme heat waves in present climate and their projection in a warming world. *Journal of Geophysical Research: Atmospheres*, 119(22):12–500.
- Satyanarayana, G. C. and Rao, D. B. (2020). Phenology of heat waves over India. *Atmospheric Research*, 245:105078.
- Schneider, U., Becker, A., Finger, P., Meyer-Christoffer, A., Rudolf, B., and Ziese, M. (2016). Gpcc full data reanalysis version 7.0: Monthly land-surface precipitation from rain gauges built on gts based and historic data.
- Seneviratne, S. I., Corti, T., Davin, E. L., Hirschi, M., Jaeger, E. B., Lehner, I., Orlowsky, B., and Teuling, A. J. (2010). Investigating soil moisture–climate interactions in a changing climate: A review. *Earth-Science Reviews*, 99(3-4):125–161.
- Srivastava, A., Rajeevan, M., and Kshirsagar, S. (2009). Development of a high resolution daily gridded temperature data set (1969–2005) for the Indian region. *Atmospheric Science Letters*, 10(4):249–254.
- Stammer, D., Köhl, A., Vlasenko, A., Matei, I., Lunkeit, F., and Schubert, S. (2018). A pilot climate sensitivity study using the CEN coupled adjoint model (CESAM). *Journal of Climate*, 31(5):2031–2056.
- Thapa, U. K., St. George, S., and Trouet, V. (2020). Poleward excursions by the Himalayan subtropical jet over the past four centuries. *Geophysical Research Letters*, 47(22):e2020GL089631.
- Vittal, H., Villarini, G., and Zhang, W. (2020). On the role of the atlantic ocean in exacerbating indian heat waves. *Climate dynamics*, 54:1887–1896.
- Vogel, M. M., Orth, R., Cheruy, F., Hagemann, S., Lorenz, R., van den Hurk, B. J., and Seneviratne, S. I. (2017). Regional amplification of projected changes in extreme temperatures strongly controlled by soil moisture-temperature feedbacks. *Geophysical Research Letters*, 44(3):1511–1519.
- Wehrli, K., Guillod, B. P., Hauser, M., Leclair, M., and Seneviratne, S. I. (2019). Identifying key driving processes of major recent heat waves. *Journal of Geophysical Research: Atmospheres*, 124(22):11746–11765.
- Yadav, R., Rupa Kumar, K., and Rajeevan, M. (2012). Characteristic features of winter precipitation and its variability over northwest India. *Journal of earth system science*, 121:611–623.
- Zuo, J., Pullen, S., Palmer, J., Bennetts, H., Chileshe, N., and Ma, T. (2015). Impacts of heat waves and corresponding measures: a review. *Journal of Cleaner Production*, 92:1–12.